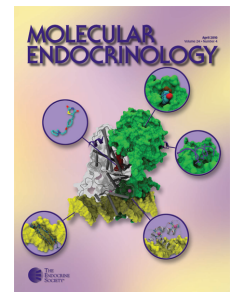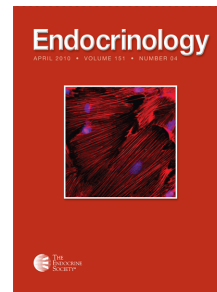# Endocrinology

Differential Effects of PPAR-{gamma} Activation versus Chemical or Genetic Reduction of DPP-4 Activity on Bone Quality in Mice

Kimberly A. Kyle, Thomas L. Willett, Laurie L. Baggio, Daniel J. Drucker and Marc D. Grynpas

Differential Effects of PPAR-γ Activation *versus* Chemical or Genetic Reduction of DPP-4 Activity on Bone Quality in Mice

Kimberly A. Kyle, Thomas L. Willett, Laurie L. Baggio, Daniel J. Drucker,* and Marc D. Grynpas*

Departments of Laboratory Medicine and Pathobiology and Medicine, Samuel Lunenfeld Research Institute, Mt. Sinai Hospital, Toronto, Ontario, Canada M5G 1X5

Patients with type 2 diabetes mellitus have an increased risk of fracture that can be further exacerbated by thiazolidinediones. A new class of antidiabetic agents control glucose through reduction of dipeptidyl peptidase-4 (DPP-4) activity; however the importance of DPP-4 for the control of bone quality has not been extensively characterized. We compared the effects of the thiazolidinedione pioglitazone and the DPP-4 inhibitor sitagliptin on bone quality in high-fat diet (HFD)-fed wild-type mice. In complementary studies, we examined bone quality in $Dpp4^{+/+}$ vs. $Dpp4^{-/-}$ mice. Pioglitazone produced yellow bones with greater bone marrow adiposity and significantly reduced vertebral bone mechanics in male, female, and ovariectomized (OVX) HFD fed female mice. Pioglitazone negatively affected vertebral volumetric bone mineral density, trabecular architecture, and mineral apposition rate in male mice. Sitagliptin treatment of HFD-fed wild-type mice significantly improved vertebral volumetric bone mineral density and trabecular architecture in female mice, but these improvements were lost in females after OVX. Genetic inactivation of $Dpp4$ did not produce a major bone phenotype in male and female $Dpp4^{-/-}$ mice; however, OVX $Dpp4^{-/-}$ mice exhibited significantly reduced femoral size and mechanics. These findings delineate the skeletal consequences of pharmacological and genetic reduction of DPP-4 activity and reveal significant differences in the effects of pioglitazone *vs.* sitagliptin *vs.* genetic $Dpp4$ inactivation on bone mechanics in mice. (*Endocrinology* 152: 457–467, 2011)

The skeleton is a highly specialized and dynamic organ that maintains bone mass by undergoing continuous remodeling over time. Osteoblastic bone formation and osteoclastic bone resorption are closely coordinated processes that enable bone to adapt to and repair the mechanical loads and age-related hormonal changes that it will endure throughout adult life. A sustained imbalance of bone formation and resorption can reduce bone quality and result in an increased susceptibility to fracture. Osteoporosis results when osteoclastic bone resorption outpaces osteoblastic bone formation leading to low bone mass, microarchitectural deterioration of the skeleton, in-

creased bone fragility, and fracture risk (1). In addition to senile or postmenopausal osteoporosis that occur with increasing age or sex steroid deficiency, patients with type 2 diabetes mellitus (T2DM) have an increased risk of fracture, despite average or elevated bone mineral density (BMD) (2–5).

Recent information demonstrates that antidiabetic agents may influence bone density and fracture rates. Long-term treatment with thiazolidinediones (TZDs) is associated with an increased risk of fracture in T2DM patients compared with treatment with other antidiabetic agents (6–9). A widely used TZD, rosiglitazone, promotes

differentiation of mesenchymal stromal cells into adipocytes rather than osteoblasts and inhibits bone formation through suppression of osteogenic transcription factors (10–14). Additionally, peroxisome proliferator-activated receptor (PPAR)-γ has been shown to have a proosteoclastogenic role and activation of PPAR-γ by rosiglitazone enhanced osteoclast differentiation in a receptor-dependent manner (15). However, not all PPAR-γ ligands exhibit the same skeletal effects, possibly due to differences in receptor binding affinity or affinity for other PPAR subtypes (16). Although pioglitazone is a widely used PPAR-γ agonist, the skeletal effects of pioglitazone treatment are much less understood. Nevertheless, the available data suggest that pioglitazone treatment leads to reduced BMD, bone formation, and mechanical strength in rodents (17).

Dipeptidyl peptidase-4 (DPP-4) inhibitors are a comparatively newer class of antidiabetic agents that improve glycemic control via enhancement of incretin hormone action (18). Several DPP-4 substrates, including glucose-dependent insulinotropic polypeptide (GIP), glucagon-like peptide (GLP)-1, and GLP-2 exert anabolic actions on the skeleton in rodents (19). However, the potential contribution of multiple DPP-4 substrates to putative changes in bone quality after DPP-4 inhibition is complex and has not been previously examined. We have now investigated and compared the effects of pioglitazone *vs.* sitagliptin on bone quality in high-fat-diet (HFD) fed male and female mice and in ovariectomized (OVX) HFD fed mice. Additionally, we evaluated bone quality in male and female and OVX $Dpp4^{-/-}$ mice.

Materials and Methods

Animals

Male and female C57BL/6 mice obtained from Taconic laboratories (Hudson, NY) were housed in the animal facility at the Toronto Centre for Phenogenomics (Toronto, Ontario, Canada). Animals were housed four to five in a cage with free access to water and food and were maintained at a constant temperature on a 12-h light, 12-h dark cycle. All mice were maintained on a standard rodent diet until 3 months of age when all mice were fed a HFD *ad libitum* (40% of kilocalories from fat; Research Diets, New Brunswick, NJ) until the animals were killed at 7 months of age. At 4 months of age, high-fat chow was supplemented with pioglitazone (Takeda Pharmaceuticals, Japan) or sitagliptin (Merck Frosst, Québec, Canada) at concentrations of 0.28 and 4 g/kg chow, respectively. The control groups were maintained on nonsupplemented high-fat chow. Selected female mice were OVX at 3 months of age and were fed chow supplemented with or without pioglitazone or sitagliptin. Lean and fat mass and water content were assessed by mouse magnetic resonance imaging as previously described (20). Similarly, oral glucose tolerance testing (1 mg glucose per gram body weight) and insulin

tolerance testing (1.2 U insulin per kilogram body weight) were carried out as described (20).

$Dpp4^{-/-}$ and $Dpp4^{+/+}$ littermate controls were generated on a C57BL/6 background as described (21). Female $Dpp4^{-/-}$ and $Dpp4^{+/+}$ mice were OVX at 3 months of age, and all mice were killed for analysis at 7 months of age. All experiments conformed to specific protocols approved by the University Health Network and Mount Sinai Hospital (Toronto, Ontario).

Preparation of bones

The right and left femora and L5 and L6 vertebrae were excised, cleaned of adherent soft tissue, and stored at −20 C in saline-soaked gauze. The processes were carefully removed from all vertebrae. Bones were thawed at room temperature before any experimental testing. The L3 and L4 vertebrae were excised and immediately fixed in 10% neutral-buffered formalin or 70% ethanol, respectively, for histomorphometry. The L3 and L4 vertebrae were allowed to fix at room temperature for 5 d before further processing for embedding purposes.

Bone mineral assessment and imaging tools

The right and left femora and L5 and L6 vertebrae were evaluated for areal BMD (aBMD; grams per square centimeter) and bone mineral content (BMC; grams) using a dual-energy x-ray absorptiometry (DEXA) PIXImus mouse densitometer (GE Medical Systems, Madison, WI) and software version 2.0. The instrument was calibrated daily using the manufacturer's phantom mouse. Bones were precisely positioned at the center of the x-ray cone beam and scanned in air on the Plexiglas platform provided. A grid on the Plexiglas platform allowed the position of each femora and vertebrae to remain consistent between samples.

Volumetric BMD (vBMD; grams per cubic centimeter) of the right femora and L5 vertebra was evaluated using a SkyScan 1174 compact microcomputed tomography machine (Micro-CT; Skyscan, Kontich, Belgium). The latter instrument was also used to evaluate the femoral geometrical properties of the right femora and trabecular architecture of the L5 vertebrae. The Skyscan CT-An software (version 1.5.0) was used for all microcomputed tomography (micro-CT) measurements and calculations (22).

Mechanical testing

Mechanical testing was performed using a 100 N load cell on an Instron 4465 testing machine (Instron Corp., Canton, MA). Load-deformation curves were generated for all mechanical tests using Labview Acquisition software (LabVIEW 5.0; National Instruments, Austin, TX). The vertebrae were tested to evaluate the lattice network of trabecular bone, whereas femora were tested to evaluate cortical bone. For three-point bending testing, each femur was positioned, posterior face down, on two supports separated by a constant 6-mm gauge length. A load was vertically applied to the midshaft of the femur at a rate of 1.0 mm/min until failure occurred. The proximal end of femora tested by three-point bending were immediately embedded in a jig with polymethyl-methacrylate and used for femoral neck fracture testing. The femoral head-neck structure was tested to failure by loading the head parallel to the shaft at a rate of 1 mm/min. For the vertebral compression testing, vertebral processes were carefully removed and L6 vertebrae were loaded at a rate of 0.5 mm/min. The distal end of the vertebral body was secured in an

upright position with cyanoacrylate-based adhesive and unilaterally compressed until a failure point or 10% drop in measured load was reached. Micro-CT and Image J analysis (National Institutes of Health, Bethesda, MD) were used to determine the geometrical properties necessary for normalization of three-point bending and vertebral compression testing, respectively (23).

Bone histomorphometry

The Leitz Bioquant morphometry system was used to quantify dynamic histomorphometry and osteoclast-staining parameters. Dynamic histomorphometry was performed to determine bone formation parameters. Two single ip injections of calcein green (0.6% caclein green; 30 mg/kg rodent) were given at 12 and 2 d before the animals were killed. L4 vertebrae were excised and immediately fixed in 70% ethanol and embedded in Spurr resin. Spurr blocks were cut in 7-μm-thick coronal sections using a Leica RM2265 rotary microtome (Leica, Wetzlar, Germany).

Tartrate-resistant acid phosphatase (TRAP)-staining for osteoclasts was performed on L3 vertebrae to quantify osteoclast numbers and surface parameters. Excised L3 vertebrae were immediately fixed in 10% buffered formalin. Samples were then decalcified using EDTA at 4 C with daily solution changes. Complete decalcification was determined by Faxitron imaging (Munich, Germany). Decalcified samples underwent processing (series of formalin, 70% ethanol, 90% ethanol, 100% ethanol, 100% xylene, and paraffin) before embedding in bone-specific paraffin. Samples were cut in 5-μm-thick coronal sections using a Leica Reichert Jung 2030 microtome (Heidelberg, Germany) and were mounted on Superfrost glass slides (Menzel-Glaser, Braunschweig, Germany). The acid phosphatase leukocyte kit and protocol (procedure no. 386; Sigma-Aldrich, St. Louis, MO) were used to prepare and perform TRAP staining.

Backscattered electron microscopy (BSE)

BSE was used for mineralization profile and strut analysis using a scanning electron microscope (Philips XL 300 SEM; Philips, Best, The Netherlands). Spurr blocks sectioned for histomorphometry were polished to a 1-μm finish. Samples were examined at a 20-kV accelerating voltage, 15-mm working distance, and a beam spot size of 6. A BSE detector (Centaurus detector) was used to image the entire polished bone surface at ×120 magnification. The backscattered signal was calibrated by observing the histogram of a silicon dioxide (SiO_2) and magnesium fluoride (MgF) standard. Gray levels represent varying degrees of bone mineralization, in which brighter intensities are indicative of increased degrees of mineralization. The mineralization profile of a specimen is represented by a histogram of gray-level intensities, and the logit function describes this mineralization distribution. Mineralization profiles were created for total (trabecular + cortical), trabecular, and cortical bone area as described (23).

Strut analysis was performed to evaluate trabecular connectivity. BSE images were digitized into binary images and skeletonized to obtain connectivity parameters. The free ends of trabeculae were described as end points; the points at which three struts met constituted nodes, and the points at which trabeculae met the cortex were designated cortical points. Parameters of connectivity included total strut length, number of nodes, length of node-node struts and node-free struts, and parameters describing disconnectivity included number of free ends and length of free-free struts (22).

Statistics

All results were analyzed using SPSS 17.0 statistical analysis software (SPSS Inc., Chicago, IL). Independent Student t tests were performed separately for sitagliptin-treated males (sitagliptin *vs.* vehicle) and pioglitazone-treated males (pioglitazone *vs.* vehicle). A one-way ANOVA was used separately for female (vehicle, sitagliptin, and pioglitazone) and OVX female (vehicle, sitagliptin, and pioglitazone) mice. Pairwise comparisons between groups were carried out using a Fisher least significant difference *post hoc* test if the group populations passed the homogeneity of variance testing. The nonparametric Dunnet's T3 *post hoc* test was performed if the variances were not homogeneous. The data were considered to be statistically significant at a confidence level of 95% ($P = 0.05$). Data are presented as mean $\pm$ SE.

Results

Metabolic effects of treatment with pioglitazone *vs.* sitagliptin

To mimic the metabolic scenario under which antidiabetic agents such as pioglitazone and sitagliptin are commonly used, we fed wild-type mice a HFD known to induce obesity, insulin resistance, and β-cell dysfunction (24). Mice maintained on a HFD supplemented with pioglitazone (HFD+PIO) gained significantly more weight (Fig. 1A) and exhibited increased body fat and relatively reduced lean body mass (Fig. 1B) compared with HFD-fed controls. In contrast, body weight gain, lean body mass, and fat content were not different between control mice and mice fed a HFD containing sitagliptin (HFD-SITA) (Fig. 1, A and B). Random blood glucose (data not shown) and levels of hemoglobin A1c were comparable in pioglitazone- *vs.* sitagliptin-treated mice (Fig. 1C). Consistent with the known mechanism of action of sitagliptin, which enhances enteral glucose tolerance through potentiation of incretin action (25), oral glucose tolerance was improved in HFD+SITA mice *vs.* controls (Fig. 1D). Likewise, blood glucose levels were lower in an insulin tolerance test in HFD+PIO mice compared with HFD-fed controls, in keeping with the insulin-sensitizing effect of pioglitazone (Fig. 1D). No differences in markers of bone formation or resorption were observed in either HFD+PIO or HFD+SITA mice compared with controls (Fig. 1E).

Effect of pioglitazone on bone quality

Bones excised from pioglitazone-treated mice appeared more yellow in color than bones from untreated or sitagliptin-treated mice (Fig. 1F). Histological analysis revealed greater bone marrow adiposity in pioglitazone-treated relative to control or sitagliptin-treated mice (Fig. 1G). DEXA revealed significant decreases in femoral aBMD of pioglitazone-treated mice, but these changes were not seen in vBMD as measured by micro-CT (Table 1). Femoral geometry, as measured by micro-CT, and fem-
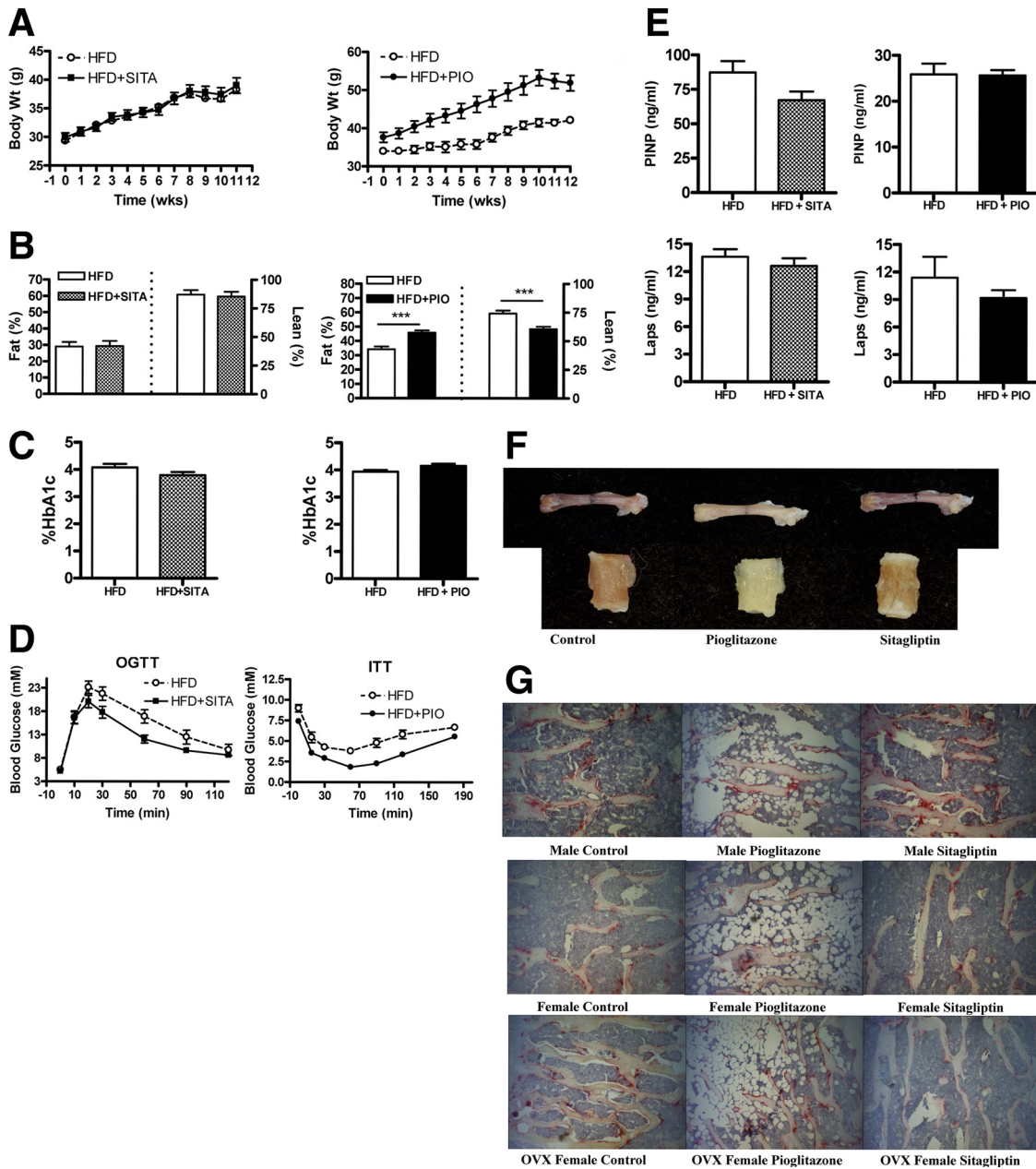
FIG. 1. Differential effects of sitagliptin *vs.* pioglitazone on metabolic parameters and bone in HFD male mice. Body weight change over time (A), body fat and lean body mass assessed by magnetic resonance imaging (B), hemoglobin A1c (HbA1c) (C), oral glucose (OGTT) or insulin tolerance testing (ITT) (D), and markers of bone formation (PINP) or resorption (Laps) (E) in wild-type male mice maintained on either a HFD or a HFD supplemented with sitagliptin (HFD+SITA) or pioglitazone (HFD+PIO) for 12 wk. Visible color change of bone (F) and increased bone marrow adiposity (TRAP staining) (G) due to pioglitazone treatment. Magnification, $\times$ 10 (n = 8–16 mice/group). For A, the AUC body weight was $P <$ 0.05 for HFD+PIO *vs.* HFD. ***, $P <$ 0.001 for HFD+PIO *vs.* HFD (B). For D, the AUC blood glucose was $P <$ 0.05 and $P <$ 0.001 for HFD+SITA or HFD+PIO, respectively, *vs.* HFD. PINP, N terminal propeptide of type I procollagen; Laps, C-telopeptide degradation products of type I collagen.

oral mechanical testing by three-point bending and femoral neck fracture testing did not reveal significant differences due to pioglitazone treatment (Supplemental Tables 1–3, published on The Endocrine Society's Journals Online web site at http://endo.endojournals.org.). Vertebral aBMD was significantly reduced in pioglitazone-treated OVX mice but was not significantly lower when measured volumetrically by micro-CT. However, pioglitazone-treated male mice exhibited significantly reduced verte-

bral vBMD (Table 1) and significantly reduced trabecular architecture (Table 2). Pioglitazone treatment produced significant reductions in trabecular bone volume (BV/TV), thickness (Tb.Th.), and number (Tb.N.) and connectivity (Table 2) with reduced total strut length, number of nodes, and length of node-node struts. Vertebral compression revealed mechanical reductions for pioglitazone-treated mice, with significant reductions in stiffness, ultimate stress, and Young's modulus for male mice; energy to fail-

TABLE 1. DEXA and micro-CT results for pioglitazone-treated and control mice

	Male		Female		OVX	
	Vehicle	**Pio**	**Vehicle**	**Pio**	**Vehicle**	**Pio**
n	8	11	8	12	9	11
Femoral aBMD (g/cm^2)	0.0586 ± 0.0015	0.0520 ± 0.0014[a]	0.0587 ± 0.0008	0.0556 ± 0.0006[a]	0.0463 ± 0.0007	0.0433 ± 0.0005[a]
Femoral BMC (g)	0.0311 ± 0.0013	0.0262 ± 0.0014[a]	0.0297 ± 0.0007	0.0275 ± 0.0004[a]	0.0191 ± 0.0006	0.0188 ± 0.0007
Femoral vBMD (g/cm^3)	1.151 ± 0.005	1.142 ± 0.005	1.182 ± 0.009	1.200 ± 0.004	1.184 ± 0.005	1.183 ± 0.005
Vertebral aBMD (g/cm^2)	0.0292 ± 0.0010	0.0263 ± 0.0010	0.0303 ± 0.0009	0.0277 ± 0.0011	0.0240 ± 0.0008	0.0207 ± 0.0003[a]
Vertebral BMC (g)	0.0023 ± 0.0002	0.0018 ± 0.0001	0.0026 ± 0.0001	0.0022 ± 0.0001	0.0015 ± 0.0001	0.0009 ± 0.0001[a]
Vertebral vBMD (g/cm^3)	0.386 ± 0.015	0.311 ± 0.019[a]	0.268 ± 0.018	0.288 ± 0.025	0.288 ± 0.025	0.247 ± 0.028

Values reported as mean ± SE. Pio, Pioglitazone.
[a] Significant ($P \leq 0.05$) compared with vehicle-treated wild-type control.

ure and toughness in female mice; and ultimate load, ultimate stress, and Young's modulus for OVX mice (Table 3). Histomorphometric analysis revealed pioglitazone treatment resulted in a significantly reduced mineral apposition rate in male mice (Supplemental Fig. 1). Quantification of osteoclast staining (Supplemental Table 4) did not reveal significant changes with the exception of reduced osteoclast number per osteoclast surface in pioglitazone-treated female mice, possibly due to increased marrow adiposity.

Effect of sitagliptin on bone quality

Sitagliptin treatment had no effect on body weight and did not affect bone color or marrow adiposity (Fig. 1, A, F, and G). Additionally, sitagliptin treatment did not affect femoral aBMD, vBMD (Table 4), geometry, or mechanical properties in male, female, or OVX mice (Supplemental Tables 5–7). Sitagliptin-treated male mice exhibited

significantly improved vertebral aBMD, but this was not significantly different when measured volumetrically by micro-CT (Table 4). Vertebral vBMD was significantly improved in sitagliptin-treated female mice despite a lack of improvement in aBMD (Table 4). No changes in BMD, volumetric or areal, were seen in sitagliptin-treated OVX mice (Table 4). Sitagliptin-treated female mice also exhibited significant improvements in trabecular architecture with increased BV/TV, Tb.Th., and Tb.N. and reduced trabecular separation (Tb.Sp.) (Table 5). Improvements in trabecular architecture were not seen in sitagliptin-treated male or OVX mice. Vertebral compression was generally not affected by sitagliptin treatment in male and female mice; however, Young's modulus was significantly decreased in sitagliptin-treated OVX mice (Supplemental Table 8). Histomorphometric analysis did not reveal significant changes in mineral apposition rate (Supplemental

TABLE 2. Vertebral trabecular architecture and connectivity for pioglitazone-treated and control mice

	Male		Female		OVX	
	Vehicle	**Pio**	**Vehicle**	**Pio**	**Vehicle**	**Pio**
n	8	11	8	12	9	11
BV/TV (%)	28.0 ± 0.8	24.1 ± 0.6[a]	19.6 ± 0.9	21.6 ± 1.5	20.5 ± 1.7	18.3 ± 1.7
Tb.Th. (μm)	65.1 ± 0.7	61.0 ± 0.9[a]	69.7 ± 1.9	67.7 ± 1.0	64.7 ± 0.7	63.7 ± 1.4
Tb.N. (mm^{-1})	4.3 ± 0.1	3.9 ± 0.1[a]	2.8 ± 0.1	3.2 ± 0.2	3.2 ± 0.3	2.8 ± 0.3
Tb.Sp. (μm)	154.9 ± 8.2	166.1 ± 5.4	250.0 ± 16.3	218.9 ± 16.5	220.0 ± 22.6	248.2 ± 23.6
n	8	11	8	11	9	11
Measures of connectivity						
Total strut length (mm/mm^2)	6.23 ± 0.17	5.63 ± 0.52[a]	4.96 ± 0.28	4.82 ± 0.30	4.19 ± 0.36	4.02 ± 0.22
Number of nodes (mm^{-2})	13.8 ± 0.9	10.7 ± 0.9[a]	12.4 ± 1.0	10.7 ± 1.0	10.6 ± 2.2	7.7 ± 0.7
Length of node-node struts (mm/mm^2)	2.49 ± 0.23	1.62 ± 0.17[a]	2.18 ± 0.34	1.66 ± 0.23	1.28 ± 0.34	0.95 ± 0.14
Length of node-free struts (mm/mm^2)	1.75 ± 0.20	1.92 ± 0.10	1.23 ± 0.15	1.39 ± 0.12	1.37 ± 0.13	1.40 ± 0.17
Measures of disconnectivity						
Number of free ends (mm^{-2})	14.8 ± 0.9	16.2 ± 0.7	9.7 ± 0.7	11.6 ± 0.7	16.2 ± 0.9	15.0 ± 0.8
Length of free-free struts (mm/mm^2)	0.45 ± 0.07	0.71 ± 0.13	0.35 ± 0.12	0.42 ± 0.08	0.62 ± 0.11	0.77 ± 0.13

Values reported as mean ± SE.
[a] Significant ($P \leq 0.05$) compared with vehicle-treated control.

TABLE 3. Vertebral compression of pioglitazone-treated and control mice

	Male		Female		OVX	
	Vehicle	Pio	Vehicle	Pio	Vehicle	Pio
n	8	10	8	12	8	10
Structural properties						
Ultimate load (n)	24.9 ± 2.5	19.8 ± 1.7	25.8 ± 2.5	22.8 ± 2.3	19.9 ± 2.1	12.5 ± 0.8[a]
Failure displacement (mm)	0.31 ± 0.03	0.38 ± 0.10	0.42 ± 0.07	0.27 ± 0.03	0.37 ± 0.05	0.38 ± 0.04
Energy to failure (mJ)	4.6 ± 0.6	4.8 ± 0.8	6.9 ± 1.4	3.4 ± 0.3[a]	4.3 ± 0.8	3.4 ± 0.57
Stiffness (N/mm)	131.0 ± 8.8	100.0 ± 9.7[a]	113.3 ± 11.1	148.9 ± 23.2	108.8 ± 17.6	66.7 ± 6.7
Material properties						
Ultimate stress (MPa)	10.7 ± 1.0	7.9 ± 0.8[a]	10.3 ± 1.1	9.7 ± 1.0	9.3 ± 1.0	5.3 ± 0.2[a]
Failure strain (%)	9.5 ± 0.9	11.7 ± 1.6	13.1 ± 2.2	8.2 ± 0.8	11.9 ± 1.6	12.3 ± 1.2
Toughness (MPa)	0.59 ± 0.07	0.57 ± 0.10	0.87 ± 0.18	0.44 ± 0.05[a]	0.64 ± 0.12	0.44 ± 0.06
Young's modulus (MPa)	183.8 ± 13.5	130.1 ± 15.1[a]	145.9 ± 15.8	209.3 ± 31.5	162.9 ± 29.2	87.9 ± 8.5[a]

Values reported as mean ± SE. MPa, Megapascals.

[a] Significant ($P \leq 0.05$) compared with vehicle-treated control.

Fig. 2) or osteoclast number due to sitagliptin treatment (Supplemental Table 9). BSE analysis of trabecular bone mineralization profiles revealed significantly increased mineralization in sitagliptin-treated male, female, and OVX mice (Supplemental Fig. 3).

Effect of genetic inactivation of DPP-4 on bone quality

Body weight was not significantly different in male or female $Dpp4^{-/-}$ *vs.* $Dpp4^{+/+}$ control mice; however, $Dpp4^{-/-}$ OVX females weighed significantly less than their OVX $Dpp4^{+/+}$ female controls (Supplemental Fig. 4). DEXA revealed significant reductions in femoral and vertebral aBMD and BMC for OVX knockout mice, but no changes were observed in male or female $Dpp4^{-/-}$ mice (Table 6). Femoral and vertebral vBMD evaluated by micro-CT did not reveal any changes in male, female, or OVX $Dpp4^{+/+}$ *vs.* $Dpp4^{-/-}$ mice (Table 6). OVX $Dpp4^{-/-}$ mice had significantly reduced femoral geometry with reductions in anterior-posterior diameter, moment of inertia, cortical thickness, and cross-sectional bone area (Table 7). Accordingly, three-point bending revealed a decrease in stiffness (Supplemental Table 10), and femoral neck fracture revealed de-

creases in ultimate load, energy to failure, and stiffness for OVX $Dpp4^{-/-}$ mice (Supplemental Table 11). No changes were seen in the femoral mechanics of male and female $Dpp4^{-/-}$ mice (Supplemental Table 11). Small changes were seen in male $Dpp4^{-/-}$ mice with reductions in vertebral ultimate load, Tb.Th. (Supplemental Tables 12 and 13 and Supplemental Fig. 6). Female $Dpp4^{-/-}$ mice exhibited an increase in vertebral Young's modulus but had reductions in Tb.N. and length of node-free strut, a measure of trabecular connectivity (Supplemental Tables 12–14). Osteoclast staining revealed no significant differences for male, female, or OVX groups (Supplemental Table 15), and no major changes were seen in the trabecular mineralization profiles (Supplemental Fig. 5) or the mineral apposition rates (Supplemental Fig. 6) across $Dpp4$ genotypes in male or female mice.

Discussion

Effects of pioglitazone treatment on bone quality

Pioglitazone treatment led to increased weight gain and marrow fat in male, female, and OVX mice. These findings

TABLE 4. DEXA and micro-CT results for sitagliptin-treated and control mice

	Male		Female		OVX	
	Vehicle	Sitagliptin	Vehicle	Sitagliptin	Vehicle	Sitagliptin
n	11	10	8	8	9	12
Femoral aBMD (g/cm²)	0.0541 ± 0.0010	0.0548 ± 0.0010	0.0587 ± 0.0008	0.0587 ± 0.0006	0.0463 ± 0.0007	0.0462 ± 0.0006
Femoral BMC (g)	0.0289 ± 0.0012	0.0311 ± 0.0011	0.0297 ± 0.0007	0.0299 ± 0.0007	0.0191 ± 0.0006	0.0198 ± 0.0004
Femoral vBMD (g/cm³)	1.090 ± 0.016	1.117 ± 0.019	1.182 ± 0.009	1.195 ± 0.010	1.184 ± 0.005	1.186 ± 0.004
Vertebral aBMD (g/cm²)	0.0258 ± 0.0009	0.0295 ± 0.0006*	0.0303 ± 0.0009	0.0321 ± 0.0011	0.0240 ± 0.0008	0.0240 ± 0.0010
Vertebral BMC (g)	0.0020 ± 0.0002	0.0028 ± 0.0001*	0.0026 ± 0.0001	0.0026 ± 0.0001	0.0015 ± 0.0001	0.0014 ± 0.0001
Vertebral vBMD (g/cm³)	0.225 ± 0.011	0.253 ± 0.012	0.268 ± 0.018	0.390 ± 0.022*	0.288 ± 0.025	0.313 ± 0.018

Values reported as mean ± SE.

* Significant ($P \leq 0.05$) compared with vehicle-treated wild-type control.

TABLE 5. Vertebral trabecular architecture for sitagliptin-treated and control mice

	Male		Female		OVX	
	Vehicle	**Sitagliptin**	**Vehicle**	**Sitagliptin**	**Vehicle**	**Sitagliptin**
n	11	10	8	8	9	11
BV/TV (%)	28.2 ± 1.1	30.8 ± 1.0	19.6 ± 0.9	27.6 ± 1.9[a]	20.5 ± 1.7	21.7 ± 1.4
Tb.Th. (μm)	71.4 ± 0.4	70.9 ± 0.6	69.7 ± 1.9	76.1 ± 1.4[a]	64.7 ± 0.7	63.9 ± 0.8
Tb.N. (mm^{-1})	3.9 ± 0.2	4.3 ± 0.1	2.8 ± 0.1	3.6 ± 0.2[a]	3.2 ± 0.3	3.4 ± 0.2
Tb.Sp. (μm)	201.3 ± 7.4	204.1 ± 6.1	250.0 ± 16.3	178.5 ± 20.6[a]	220.0 ± 22.6	190.6 ± 19.8

Values reported as mean ± SE.
[a] Significant (P ≤ 0.05) compared with vehicle-treated control.

are consistent with previous reports of weight gain and increased bone marrow fat (13, 14, 26) associated with TZD treatment. Pioglitazone-treated male, female, and OVX mice experienced significant reductions in femoral aBMD and BMC; however, these changes were not seen when femoral BMD was measured volumetrically by micro-CT. Additionally, no changes were seen in the femoral geometry or mechanics of pioglitazone-treated mice. The lack of changes seen in femoral mechanics were unexpected, given reports of fractures of the distal upper and lower limbs and not of the spine in human subjects exposed to TZDs for several years (7, 27, 28). Because cortical bone has a lower surface area and overall slower turnover rate than trabecular bone, a longer treatment period may be required to detect greater effects of pioglitazone on the skeleton. Consistent with this possibility, reductions in three-point bending mechanics were detected in rats treated with a higher dose of pioglitazone for 4 months, yet no changes were seen in femoral neck fractures (17).

Although pioglitazone negatively affected vertebral mechanics of all treated mice, male mice exhibited the greatest sensitivity to the metabolic and skeletal effects of pioglitazone with reductions in trabecular architecture and connectivity as well as reduced bone formation. The results obtained here with pioglitazone are consistent with observations reporting reductions in vertebral strength (29), trabecular architecture (13, 29), and mineral apposition (13, 29) in male mice treated with rosiglitazone.

Pioglitazone-treated female mice did not exhibit changes in vertebral vBMD, trabecular architecture, and connectivity, suggesting that the reductions in vertebral mechanics are not likely due to adverse effects on bone mineral. Energy to failure and toughness are largely influenced by collagen and not necessarily by changes in the mineral phase or density of bone (30–32). Furthermore, no significant changes were seen in bone formation parameters in female mice treated with pioglitazone. This finding was unexpected, given that clinical studies revealed an increased risk of fracture in women treated with pioglitazone (27, 28, 33). However, a study by Sottile *et al.* (34) reported a dissociation between the doses of rosiglitazone required to generate metabolic effects without producing significant differences in BMD or histomorphometric parameters in female rats. The reductions in energy to failure and toughness in pioglitazone-treated female mice are consistent with negative effects on the collagen network (30, 31). Interestingly, TZD activation of PPAR-γ resulted in suppression of type 1 collagen in a stromal cell line (10), and PPAR-γ-mediated reductions in collagen biosynthesis are dependent on levels of estrogen (35, 36). Nevertheless, the effects of PPAR-γ activation on collagen and bone strength are not fully understood.

TABLE 6. DEXA and micro-CT results for *Dpp4*$^{-/-}$ (KO) and WT mice

	Male		Female		OVX	
	WT	**KO**	**WT**	**KO**	**WT**	**KO**
n	15	23	14	19	10	13
Femoral aBMD (g/cm^2)	0.0548 ± 0.0009	0.0523 ± 0.0010	0.0538 ± 0.0007	0.0547 ± 0.0010	0.0498 ± 0.0011	0.0446 ± 0.0004[a]
Femoral BMC (g)	0.0276 ± 0.0008	0.0263 ± 0.0008	0.0251 ± 0.0006	0.0263 ± 0.0008	0.0240 ± 0.0007	0.0197 ± 0.0003[a]
Femoral vBMD (g/cm^3)	1.264 ± 0.008	1.259 ± 0.006	1.285 ± 0.006	1.273 ± 0.004	1.265 ± 0.005	1.251 ± 0.026
Vertebral aBMD (g/cm^2)	0.0267 ± 0.0009	0.0247 ± 0.0007	0.0262 ± 0.0009	0.0272 ± 0.0007	0.0203 ± 0.0012	0.0150 ± 0.0010[a]
Vertebral BMC (g)	0.0020 ± 0.0002	0.0017 ± 0.0001	0.0019 ± 0.0002	0.0021 ± 0.0001	0.0011 ± 0.0001	0.0005 ± 0.0001[a]
Vertebral vBMD (g/cm^3)	0.265 ± 0.020	0.265 ± 0.011	0.279 ± 0.022	0.265 ± 0.013	0.292 ± 0.022	0.260 ± 0.015

Values reported as mean ± SE. WT, Wild type; KO, knockout.
[a] Significant (*P* ≤ 0.05) compared with wild-type control.

TABLE 7. Geometrical properties of right femora for *Dpp4*$^{-/-}$ (KO) and WT mice

	Male		Female		OVX	
	WT	**KO**	**WT**	**KO**	**WT**	**KO**
n	15	23	14	18	10	13
A-P diameter (mm)	1.38 ± 0.02	1.42 ± 0.02	1.35 ± 0.01	1.36 ± 0.01	1.39 ± 0.01	1.33 ± 0.01[a]
Moment of inertia (mm^4)	0.173 ± 0.011	0.177 ± 0.007	0.141 ± 0.004	0.147 ± 0.005	0.155 ± 0.007	0.120 ± 0.003[a]
Cross-sectional bone area (mm^2)	0.895 ± 0.022	0.877 ± 0.016	0.849 ± 0.017	0.847 ± 0.016	0.808 ± 0.028	0.688 ± 0.016[a]
Cortical thickness (mm)	0.173 ± 0.009	0.166 ± 0.003	0.182 ± 0.003	0.183 ± 0.003	0.167 ± 0.005	0.151 ± 0.004[a]

Values reported as mean ± SE. WT, Wild type; KO, knockout; A-P, anterior-posterior.

[a] Significant (P ≤ 0.05) compared with wild-type control.

Effects of sitagliptin on bone quality

We originally hypothesized that sitagliptin may produce positive effects on bone due to its regulation of multiple gut hormones such as GIP and GLP-2, known to enhance bone formation and/or prevent bone resorption (37). The GIP receptor is expressed in osteoblasts (38), and GIP increased collagen type 1 expression and alkaline phosphatase activity in osteoblast-like cells (38) as well as protected osteoblasts from apoptosis (39). GIP receptors have also been found on osteoclasts and GIP inhibits bone resorption *in vitro* (40). *Gipr*$^{-/-}$ mice exhibit low bone mass due to decreased bone formation and increased bone resorption (39, 41).

The proglucagon-derived peptide, GLP-2, is also a DPP-4 substrate (42, 43). Exogenous GLP-2 administration reduced serum and urine markers of bone resorption and increased hip BMD in a dose-dependent manner in postmenopausal women and improved spinal BMD in short-bowel patients with no colon (44–46). The skeletal role of the proglucagon-derived peptide, GLP-1, cosecreted together with GLP-2, is less understood, but the GLP-1 receptor is expressed in rodent thyroid C cells, and GLP-1 increases calcitonin secretion and gene expression in mice and rats (47, 48). *Glp1r*$^{-/-}$ mice exhibit cortical osteopenia and reduced levels of calcitonin, suggesting that GLP-1 may have an indirect role in murine bone metabolism, possibly through a calcitonin-mediated pathway (48).

Female mice treated with sitagliptin exhibited significant improvements in vertebral vBMD and trabecular architecture. Whether these positive changes reflect the cumulative actions of GIP, GLP-1, and GLP-2, or actions of sitagliptin on other substrates acting on the skeleton, cannot be determined from the present study. The improvements seen in vertebral vBMD and trabecular architecture in female mice were lost in sitagliptin-treated OVX female mice, suggesting that partial DPP-4 inhibition does not offset the adverse skeletal effects arising from a marked decline in estrogen production. The beneficial effects seen with sitagliptin treatment in female mice were not seen in male mice.

Interestingly, BSE analysis of total and trabecular bone area mineralization profiles revealed significant shifts toward increased mineralization for all sitagliptin-treated mice, independent of gender or OVX. These increases suggest that inhibition of DPP-4 activity reduces the resorptive rate of bone. GLP-2 administration has been associated with an acute suppression in bone resorption based on bone marker evaluation (49). Suppressed bone resorption could allow more time for secondary mineralization to occur, resulting in a more mineralized bone. Another explanation for increased mineralization could be improved calcium deposition on bone, which may be linked to GIP action (39). Taken together, sitagliptin treatment appears to have a neutral effect on femoral bone mechanics in mice with only modest effects on vertebral bone mechanics. Because we cannot completely exclude the possibility that sitagliptin may exert effects on bone independent of its inhibition of DPP-4 catalytic activity, attribution of these results to the DPP-4-inhibitory properties of sitagliptin will require additional studies using chemically distinct DPP-4 inhibitors.

Effects of genetic inactivation of DPP-4 on bone quality

Sitagliptin treatment reduces but does not completely abrogate DPP-4 activity; hence, we assessed bone quality in mice with complete genetic disruption of the *Dpp4* gene to identify a potential skeletal role for the transmembrane or soluble forms of DPP-4. Because *Dpp4*$^{-/-}$ mice are resistant to HFD-induced obesity (50), we studied *Dpp4*$^{-/-}$ mice fed a regular chow diet to avoid the confounding effects of differential weight gain in the analysis of bone quality. Genetic inactivation of *Dpp4* results in modest defects in bone quality in male and female mice. Male *Dpp4*$^{-/-}$ mice exhibited significantly reduced ultimate load, Tb.Th. and mineral apposition rate, whereas female *Dpp4*$^{-/-}$ mice exhibited significantly reduced

Tb.N. and length of node-free strut (a measure of connectivity) but exhibited a significantly increased vertebral Young's modulus. It is important to note that the skeletal changes seen in male and female $Dpp4^{-/-}$ mice were quite modest, given the wide range of tests performed to quantify bone quality. The majority of analyses found no significant differences comparing male and female $Dpp4^{+/+}$ vs. $Dpp4^{-/-}$ mice, demonstrating that genetic inactivation of $Dpp4$ does not produce a striking bone phenotype in normal mice.

On the other hand, $Dpp4^{-/-}$ OVX mice exhibited reductions in femoral geometry and femoral structural properties. The interpretation of these data is complicated by the observation that $Dpp4^{-/-}$ mice gain less weight after OVX relative to their $Dpp4^{+/+}$ littermate controls. Weight gain is an undesirable and complicating effect of OVX in rodent models because it provides partial protection against OVX-induced bone loss (51). Interestingly, the positive effects of sitagliptin treatment on bone quality in female mice were lost in sitagliptin-treated OVX mice, and sitagliptin treatment was associated with less weight gain compared with non-sitagliptin-treated OVX controls. Hence, the effects of DPP-4 inhibition on prevention of weight gain may partially offset the positive effects of DPP-4 inhibition on potentiation of gut hormone action in a postmenopausal estrogen-deficient model.

The motivation for examining the effects of DPP-4 inhibition on the skeleton was partly based on studies that suggested positive skeletal effects from gut hormones that are also DPP-4 substrates, principally GIP, GLP-1, GLP-2, and peptide YY. Nevertheless, the anabolic and antiresorptive effects of gut hormones have usually been demonstrated in studies administering pharmacological doses of gut hormones (49), whereas DPP-4 inhibition and genetic inactivation of $Dpp4$ would be expected to produce only modest changes in the levels of active gut hormones. Direct comparison of the phenotypes arising in mice treated with sitagliptin vs. $Dpp4^{-/-}$ mice is difficult for several reasons. First, sitagliptin-treated mice were studied on a HFD known to produce multiple changes in insulin secretion, insulin action, and levels of circulating adipokines, independent metabolic parameters that may also influence bone quality. Furthermore, sitgaliptin produces partial but incomplete reduction of DPP-4 activity, whereas $Dpp4^{-/-}$ mice exhibit complete disruption of enzyme activity and the potential for compensatory changes in related genes and proteins that may mask a skeletal phenotype. Nevertheless, mice subjected to DPP-4 inhibition with sitagliptin and $Dpp4^{-/-}$ mice exhibit only modest skeletal phenotypes, notably increasing mineralization and skeletal effects that are reduced in females after OVX.

In summary, pioglitazone negatively affects trabecular bone mechanics in male and female wild-type mice and in estrogen-deficient OVX mice, whereas sitagliptin produces very few changes in bone quality. Although TZDs also increase fracture risk in human subjects, it is difficult to extrapolate results obtained with sitagliptin in studies of rodent bone quality to human subjects due to species-specific differences in skeletal and gut hormone biology. For example, although both $Gipr^{-/-}$ and $Glp1r^{-/-}$ mice exhibit skeletal phenotypes, and exogenous administration of GIP and GLP-1 reduce bone resorption in rodents, acute administration of GIP or GLP-1 has no effect on markers of bone turnover in human subjects (39, 47–49, 52, 53). Nevertheless, because T2DM is a chronic disease associated with reduced bone quality and an increased risk of bone fractures, additional studies examining the effects of antidiabetic agents potentiating incretin action on bone formation, quality, and resorption are clearly warranted.

Acknowledgments

References

1. **Manolagas SC** 2000 Birth and death of bone cells: basic regulatory mechanisms and implications for the pathogenesis and treatment of osteoporosis. Endocr Rev 21:115–137
2. **de Liefde I, van der Klift M, de Laet CE, van Daele PL, Hofman A, Pols HA** 2005 Bone mineral density and fracture risk in type-2 diabetes mellitus: the Rotterdam Study. Osteoporos Int 16:1713–1720
3. **Hofbauer LC, Brueck CC, Singh SK, Dobnig H** 2007 Osteoporosis in patients with diabetes mellitus. J Bone Miner Res 9:1317–1328
4. **Kwon DJ, Kim JH, Chung KW, Lee JW, Kim SP, Lee HY** 1996 Bone mineral density of the spine using dual energy X-ray absorptiometry in patients with non-insulin-dependent diabetes mellitus. J Obstet Gynaecol Res 22:157–162

5. **Strotmeyer ES, Cauley JA, Schwartz AV, Nevitt MC, Resnick HE, Zmuda JM, Bauer DC, Tylavsky FA, de Rekeneire N, Harris TB, Newman AB** 2004 Diabetes is associated independently of body composition with BMD and bone volume in older white and black men and women: the Health, Aging, and Body Composition Study. J Bone Miner Res 19:1084–1091

6. **Grey A, Bolland M, Gamble G, Wattie D, Horne A, Davidson J, Reid IR** 2007 The peroxisome-proliferator-activated receptor-γ agonist rosiglitazone decreases bone formation and bone mineral density in healthy postmenopausal women: a randomized, controlled trial. J Clin Endocrinol Metab 92:1305–1310

7. **Kahn SE, Zinman B, Lachin JM, Haffner SM, Herman WH, Holman RR, Kravitz BG, Yu D, Heise MA, Aftring RP, Viberti G** 2008 Rosiglitazone associated fractures in type 2 diabetes: an analysis from ADOPT. Diabetes Care 31:845–851

8. **Schwartz AV, Sellmeyer DE, Vittinghoff E, Palermo L, Lecka-Czernik B, Feingold KR, Strotmeyer ES, Resnick HE, Carbone L, Beamer BA, Park SW, Lane NE, Harris TB, Cummings SR** 2006 Thiazolidinedione use and bone loss in older diabetic adults. J Clin Endocrinol Metab 91:3349–3354

9. **Meier C, Kraenzlin ME, Bodmer M, Jick SS, Jick H, Meier CR** 2008 Use of thiazolidinediones and fracture risk. Arch Intern Med 168:820–825

10. **Lecka-Czernik B, Gubrij I, Moerman EJ, Kajkenova O, Lipschitz DA, Manolagas SC, Jilka RL** 1999 Inhibition of Osf2/Cbfa1 expression and terminal osteoblast differentiation by PPARγ2. J Cell Biochem 74:357–371

11. **Lecka-Czernik B, Moerman EJ, Grant DF, Lehmann JM, Manolagas SC, Jilka RL** 2002 Divergent effects of selective peroxisome proliferator-activated receptor-γ 2 ligands on adipocyte versus osteoblast differentiation. Endocrinology 143:2376–2384

12. **Ali AA, Weinstein RS, Stewart SA, Parfitt AM, Manolagas SC, Jilka RL** 2005 Rosiglitazone causes bone loss in mice by suppressing osteoblast differentiation and bone formation. Endocrinology 146:1226–1235

13. **Rzonca SO, Suva LJ, Gaddy D, Montague DC, Lecka-Czernik B** 2004 Bone is a target for the antidiabetic compound rosiglitazone. Endocrinology 145:401–406

14. **Lazarenko OP, Rzonca SO, Suva LJ, Lecka-Czernik B** 2006 Netoglitazone is a PPAR-γ ligand with selective effects on bone and fat. Bone 38:74–84

15. **Wan Y, Chong LW, Evans RM** 2007 PPAR-γ regulates osteoclastogenesis in mice. Nat Med 13:1496–1503

16. **Gimble JM, Zvonic S, Floyd ZE, Kassem M, Nuttall ME** 2006 Playing with bone and fat. J Cell Biochem 98:251–266

17. **Syversen U, Stunes AK, Gustafsson BI, Obrant KJ, Nordsletten L, Berge R, Thommesen L, Reseland JE** 2009 Different skeletal effects of the peroxisome proliferator activated receptor (PPAR)α agonist fenofibrate and the PPARγ agonist pioglitazone. BMC Endocr Disord 9:10

18. **Drucker DJ, Nauck MA** 2006 The incretin system: glucagon-like peptide-1 receptor agonists and dipeptidyl peptidase-4 inhibitors in type 2 diabetes. Lancet 368:1696–1705

19. **Walsh JS, Henriksen DB** 2010 Feeding and bone. Arch Biochem Biophys 503:11–19

20. **Hansotia T, Maida A, Flock G, Yamada Y, Tsukiyama K, Seino Y, Drucker DJ** 2007 Extrapancreatic incretin receptors modulate glucose homeostasis, body weight, and energy expenditure. J Clin Invest 117:143–152

21. **Marguet D, Baggio L, Kobayashi T, Bernard AM, Pierres M, Nielsen PF, Ribel U, Watanabe T, Drucker DJ, Wagtmann N** 2000 Enhanced insulin secretion and improved glucose tolerance in mice lacking CD26. Proc Natl Acad Sci USA 97:6874–6879

22. **Magalhaes JK, Grynpas MD, Willett TL, Glogauer M** Deleting Rac1 improves vertebral bone quality and resistance to fracture in a murine ovariectomy model. Osteoporos Int 10.1007/s00198-010-1355-6

23. **Mousny M, Omelon S, Wise L, Everett ET, Dumitriu M, Holmyard DP, Banse X, Devogelaer JP, Grynpas MD** 2008 Fluoride effects on bone formation and mineralization are influenced by genetics. Bone 43:1067–1074

24. **Winzell MS, Ahren B** 2004 The high-fat diet-fed mouse: a model for studying mechanisms and treatment of impaired glucose tolerance and type 2 diabetes. Diabetes 53(Suppl 3):S215–S219

25. **Hansotia T, Baggio LL, Delmeire D, Hinke SA, Yamada Y, Tsukiyama K, Seino Y, Holst JJ, Schuit F, Drucker DJ** 2004 Double incretin receptor knockout (DIRKO) mice reveal an essential role for the enteroinsular axis in transducing the glucoregulatory actions of DPP-IV inhibitors. Diabetes 53:1326–1335

26. **Soroceanu MA, Miao D, Bai XY, Su H, Goltzman D, Karaplis AC** 2004 Rosiglitazone impacts negatively on bone by promoting osteoblast/osteocyte apoptosis. J Endocrinol 183:203–216

27. **Bilik D, McEwen LN, Brown MB, Pomeroy NE, Kim C, Asao K, Crosson JC, Duru OK, Ferrara A, Hsiao VC, Karter AJ, Lee PG, Marrero DG, Selby JV, Subramanian U, Herman WH** 2010 Thiazolidinediones and fractures: evidence from translating research into action for diabetes. J Clin Endocrinol Metab 95:4560–4565

28. **Aubert RE, Herrera V, Chen W, Haffner SM, Pendergrass M** 2010 Rosiglitazone and pioglitazone increase fracture risk in women and men with type 2 diabetes. Diabetes Obes Metab 12:716–721

29. **Lazarenko OP, Rzonca SO, Hogue WR, Swain FL, Suva LJ, Lecka-Czernik B** 2007 Rosiglitazone induces decreases in bone mass and strength that are reminiscent of aged bone. Endocrinology 148:2669–2680

30. **Wang X, Bank RA, TeKoppele JM, Hubbard GB, Athanasiou KA, Agrawal CM** 2000 Effect of collagen denaturation on the toughness of bone. Clin Orthop Relat Res 371:228–239

31. **Wang X, Shen X, Li X, Agrawal CM** 2002 Age-related changes in the collagen network and toughness of bone. Bone 31:1–7

32. **Wang XD, Masilamani NS, Mabrey JD, Alder ME, Agrawal CM** 1998 Changes in the fracture toughness of bone may not be reflected in its mineral density, porosity, and tensile properties. Bone 23:67–72

33. **Loke YK, Singh S, Furberg CD** 2009 Long-term use of thiazolidinediones and fractures in type 2 diabetes: a meta-analysis. CMAJ 180:32–39

34. **Sottile V, Seuwen K, Kneissel M** 2004 Enhanced marrow adipogenesis and bone resorption in estrogen-deprived rats treated with the PPARγ agonist BRL49653 (rosiglitazone). Calcif Tissue Int 75:329–337

35. **Kociecka B, Surazynski A, Miltyk W, Palka J** 2010 The effect of Telmisartan on collagen biosynthesis depends on the status of estrogen activation in breast cancer cells. Eur J Pharmacol 628:51–56

36. **Surazynski A, Jarzabek K, Miltyk W, Wolczynski S, Palka J** 2009 Estrogen-dependent regulation of PPAR-γ signaling on collagen biosynthesis in adenocarcinoma endometrial cells. Neoplasma 56:448–454

37. **Drucker DJ** 2007 Dipeptidyl peptidase-4 inhibition and the treatment of type 2 diabetes: preclinical biology and mechanisms of action. Diabetes Care 30:1335–1343

38. **Bollag RJ, Zhong Q, Phillips P, Min L, Zhong L, Cameron R, Mulloy AL, Rasmussen H, Qin F, Ding KH, Isales CM** 2000 Osteoblast-derived cells express functional glucose-dependent insulinotropic peptide receptors. Endocrinology 141:1228–1235

39. **Tsukiyama K, Yamada Y, Yamada C, Harada N, Kawasaki Y, Ogura M, Bessho K, Li M, Amizuka N, Sato M, Udagawa N, Takahashi N, Tanaka K, Oiso Y, Seino Y** 2006 Gastric inhibitory polypeptide as an endogenous factor promoting new bone formation after food ingestion. Mol Endocrinol 20:1644–1651

40. **Zhong Q, Itokawa T, Sridhar S, Ding KH, Xie D, Kang B, Bollag WB, Bollag RJ, Hamrick M, Insogna K, Isales CM** 2007 Effects of glucose-dependent insulinotropic peptide on osteoclast function. Am J Physiol Endocrinol Metab 292:E543–E548

41. **Xie D, Cheng H, Hamrick M, Zhong Q, Ding KH, Correa D, Williams S, Mulloy A, Bollag W, Bollag RJ, Runner RR, McPherson JC, Insogna K, Isales CM** 2005 Glucose-dependent insulinotropic

polypeptide receptor knockout mice have altered bone turnover. Bone 37:759–769

42. **Drucker DJ, Shi Q, Crivici A, Sumner-Smith M, Tavares W, Hill M, DeForest L, Cooper S, Brubaker PL** 1997 Regulation of the biological activity of glucagon-like peptide 2 *in vivo* by dipeptidyl peptidase IV. Nat Biotechnol 15:673–677

43. **Hartmann B, Thulesen J, Kissow H, Thulesen S, Orskov C, Ropke C, Poulsen SS, Holst JJ** 2000 Dipeptidyl peptidase IV inhibition enhances the intestinotrophic effect of glucagon-like peptide-2 in rats and mice. Endocrinology 141:4013–4020

44. **Haderslev KV, Jeppesen PB, Hartmann B, Thulesen J, Sorensen HA, Graff J, Hansen BS, Tofteng F, Poulsen SS, Madsen JL, Holst JJ, Staun M, Mortensen PB** 2002 Short-term administration of glucagon-like peptide-2. Effects on bone mineral density and markers of bone turnover in short-bowel patients with no colon. Scand J Gastroenterol 37:392–398

45. **Henriksen DB, Alexandersen P, Byrjalsen I, Hartmann B, Bone HG, Christiansen C, Holst JJ** 2004 Reduction of nocturnal rise in bone resorption by subcutaneous GLP-2. Bone 34:140–147

46. **Henriksen DB, Alexandersen P, Hartmann B, Adrian CL, Byrjalsen I, Bone HG, Holst JJ, Christiansen C** 2009 Four-month treatment with GLP-2 significantly increases hip BMD: a randomized, placebo-controlled, dose-ranging study in postmenopausal women with low BMD. Bone 45:833–842

47. **Bjerre Knudsen L, Madsen LW, Andersen S, Almholt K, de Boer AS, Drucker DJ, Gotfredsen C, Egerod FL, Hegelund AC, Jacobsen H, Jacobsen SD, Moses AC, Molck AM, Nielsen HS, Nowak J, Solberg H, Thi TD, Zdravkovic M** 2010 Glucagon-like peptide-1 receptor agonists activate rodent thyroid C-cells causing calcitonin release and C-cell proliferation. Endocrinology 151:1473–1486

48. **Yamada C, Yamada Y, Tsukiyama K, Yamada K, Udagawa N, Takahashi N, Tanaka K, Drucker DJ, Seino Y, Inagaki N** 2008 The murine glucagon-like peptide-1 receptor is essential for control of bone resorption. Endocrinology 149:574–579

49. **Henriksen DB, Alexandersen P, Bjarnason NH, Vilsboll T, Hartmann B, Henriksen EE, Byrjalsen I, Krarup T, Holst JJ, Christiansen C** 2003 Role of gastrointestinal hormones in postprandial reduction of bone resorption. J Bone Miner Res 18:2180–2189

50. **Conarello SL, Li Z, Ronan J, Roy RS, Zhu L, Jiang G, Liu F, Woods J, Zycband E, Moller DE, Thornberry NA, Zhang BB** 2003 Mice lacking dipeptidyl peptidase IV are protected against obesity and insulin resistance. Proc Natl Acad Sci USA 100:6825–6830

51. **Wronski TJ, Schenck PA, Cintrón M, Walsh CC** 1987 Effect of body weight on osteopenia in ovariectomized rats. Calcif Tissue Int 40:155–159

52. **Bollag RJ, Zhong Q, Ding KH, Phillips P, Zhong L, Qin F, Cranford J, Mulloy AL, Cameron R, Isales CM** 2001 Glucose-dependent insulinotropic peptide is an integrative hormone with osteotropic effects. Mol Cell Endocrinol 177:35–41

53. **Xie D, Zhong Q, Ding KH, Cheng H, Williams S, Correa D, Bollag WB, Bollag RJ, Insogna K, Troiano N, Coady C, Hamrick M, Isales CM** 2007 Glucose-dependent insulinotropic peptide-overexpressing transgenic mice have increased bone mass. Bone 40:1352–1360

Supplemental Table 1. Geometrical properties of right femora for pioglitazone-treated and control mice

	Male		Female		OVX	
	Vehicle	Pio	Vehicle	Pio	Vehicle	Pio
n	8	11	8	12	9	11
A-P Diameter (mm)	1.37 ± 0.03	1.32 ± 0.03	1.29 ± 0.01	1.29 ± 0.02	1.32 ± 0.02	1.29 ± 0.01
Moment of Inertia (mm^4)	0.244 ± 0.020	0.210 ± 0.024	0.189 ± 0.005	0.189 ± 0.005	0.177 ± 0.006	0.191 ± 0.007
Cross-sectional bone area (mm^2)	1.16 ± 0.02	1.06 ± 0.05	1.10 ± 0.01	1.10 ± 0.02	0.99 ± 0.02	0.98 ± 0.02
Cortical Thickness (mm)	0.210 ± 0.003	0.201 ± 0.003	0.231 ± 0.002	0.236 ± 0.002	0.205 ± 0.004	0.200 ± 0.004

Values reported as mean ± standard error.

Supplemental Table 2. Femoral three-point bending results for pioglitazone-treated and control mice

	Male		Female		OVX	
	Vehicle	**Pio**	**Vehicle**	**Pio**	**Vehicle**	**Pio**
n	**8**	**10**	**8**	**12**	**9**	**11**
Structural Properties						
Ultimate Load (N)	20.3 ± 0.9	18.3 ± 0.6	24.5 ± 0.7	24.8 ± 0.9	16.3 ± 1.3	16.1 ± 1.0
Failure Displacement (mm)	0.55 ± 0.09	0.58 ± 0.06	0.43 ± 0.04	0.40 ± 0.03	0.30 ± 0.03	0.44 ± 0.08
Energy to Failure (mJ)	8.2 ± 1.1	7.5 ± 0.8	7.3 ± 0.8	6.7 ± 0.4	3.2 ± 0.6	4.5 ± 0.8
Stiffness (N/mm)	152.5 ± 6.4	137.8 ± 8.9	177.2 ± 5.5	165.1 ± 8.1	149.5 ± 5.5	149.7 ± 5.2
Material Properties						
Ultimate Stress (MPa)	87.4 ± 4.2	94.8 ± 4.2	125.5 ± 5.8	126.8 ± 3.1	91.3 ± 6.1	92.5 ± 7.7
Failure Strain (%)	12.5 ± 1.9	12.6 ± 1.6	9.1 ± 0.9	8.5 ± 0.6	6.6 ± 0.7	9.5 ± 1.7
Toughness (MPa)	7.9 ± 1.0	8.3 ± 0.9	8.0 ± 0.9	7.4 ± 0.5	3.8 ± 0.7	4.8 ± 1.1
Young's Modulus (MPa)	2905.8 ± 184.2	3420.0 ± 357.9	4224.9 ± 151.8	3923.5 ± 166.4	3820.3 ± 114.0	4035.4 ± 347.6

Values reported as mean $\pm$ standard error.

Supplemental Table 3. Femoral neck fracture results for pioglitazone-treated and control mice

	Male		Female		OVX	
	Vehicle	Pio	Vehicle	Pio	Vehicle	Pio
n	8	11	8	12	9	11
Structural Properties						
Ultimate Load (N)	26.3 ± 2.8	22.0 ± 1.4	21.5 ± 0.8	21.0 ± 1.3	15.9 ± 1.3	17.0 ± 0.9
Failure Displacement (mm)	0.26 ± 0.04	0.28 ± 0.03	0.21 ± 0.02	0.23 ± 0.02	0.22 ± 0.03	0.25 ± 0.03
Energy to Failure (mJ)	3.7 ± 0.6	3.8 ± 0.5	2.8 ± 0.3	3.1 ± 0.4	2.1 ± 0.4	2.5 ± 0.3
Stiffness (N/mm)	146.7 ± 12.8	130.7 ± 10.8	136.4 ± 12.7	136.2 ± 8.3	105.5 ± 10.6	102.5 ± 8.8

Values reported as mean ± standard error.

Supplemental Table 4. Osteoclast staining in pioglitazone-treated and control mice

	Male		Female		OVX	
	Vehicle	Pio	Vehicle	Pio	Vehicle	Pio
n	7	11	8	12	9	11
Number of Osteoclasts (-)	43 ± 5	56 ± 5	64 ± 6	64 ± 5	45 ± 4	36 ± 4
Osteoclast Surface (mm)	0.99 ± 0.16	1.12 ± 0.09	1.28 ± 0.10	1.67 ± 0.16	0.93 ± 0.11	0.76 ± 0.09
Percent Osteoclast Surface (%)	8.2 ± 1.5	9.0 ± 0.7	13.4 ± 1.8	17.3 ± 1.7	10.1 ± 1.4	9.8 ± 1.0
Number of Osteoclasts per Bone Surface (mm^{-1})	3.5 ± 0.4	4.5 ± 0.3	6.7 ± 1.0	6.6 ± 0.4	4.9 ± 0.5	4.6 ± 0.5
Number of Osteoclasts per Osteoclast Surface	45.8 ± 2.9	50.5 ± 2.4	50.5 ± 4.6	39.5 ± 1.6*	52.5 ± 5.9	48.6 ± 3.9

*Values reported as mean ± standard error. * Significant ($p \leq 0.05$) compared to vehicle-treated controls*

Supplemental Table 5. Geometrical properties of right femora for sitagliptin-treated and control vehicle-treated mice

	Male		Female		OVX	
	Vehicle	Sitagliptin	Vehicle	Sitagliptin	Vehicle	Sitagliptin
n	11	10	8	8	9	12
A-P Diameter (mm)	1.30 ± 0.03	1.31 ± 0.02	1.29 ± 0.01	1.32 ± 0.02	1.32 ± 0.02	1.30 ± 0.01
Moment of Inertia (mm^4)	0.158 ± 0.011	0.165 ± 0.010	0.189 ± 0.005	0.198 ± 0.005	0.177 ± 0.006	0.184 ± 0.006
Cross-sectional bone area (mm^2)	0.87 ± 0.02	0.99 ± 0.10	1.10 ± 0.01	1.12 ± 0.02	0.99 ± 0.02	0.97 ± 0.01
Cortical Thickness (mm)	0.167 ± 0.012	0.168 ± 0.003	0.231 ± 0.002	0.234 ± 0.003	0.205 ± 0.004	0.200 ± 0.003

Values reported as mean ± standard error.

Supplemental Table 6. Femoral three-point bending results for sitagliptin-treated and vehicle-treated control mice

	Male		Female		OVX	
	Vehicle	Sitagliptin	Vehicle	Sitagliptin	Vehicle	Sitagliptin
n	11	10	8	8	9	12
Structural Properties						
Ultimate Load (N)	17.7 ± 0.6	17.9 ± 0.6	24.5 ± 0.7	23.6 ± 0.9	16.3 ± 1.3	17.3 ± 0.5
Failure Displacement (mm)	0.51 ± 0.07	0.53 ± 0.06	0.43 ± 0.04	0.53 ± 0.08	0.30 ± 0.03	0.33 ± 0.04
Energy to Failure (mJ)	6.1 ± 0.8	6.3 ± 0.7	7.3 ± 0.8	7.8 ± 0.9	3.2 ± 0.6	3.7 ± 0.5
Stiffness (N/mm)	123.7 ± 5.8	129.0 ± 3.7	177.2 ± 5.5	179.6 ± 10.9	149.5 ± 5.5	144.9 ± 4.2
Material Properties						
Ultimate Stress (MPa)	124.4 ± 7.2	114.3 ± 3.2	94.4 ± 5.8	117.8 ± 4.6	91.3 ± 6.1	92.2 ± 3.3
Failure Strain (%)	10.6 ± 1.4	11.6 ± 1.3	9.1 ± 0.9	11.6 ± 1.7	6.6 ± 0.7	7.1 ± 0.8
Toughness (MPa)	9.2 ± 1.3	8.7 ± 0.9	8.0 ± 0.9	8.7 ± 1.1	3.8 ± 0.7	4.3 ± 0.6
Young's Modulus (MPa)	4205.4 ± 391.4	3784.2 ± 154.4	4224.9 ± 151.8	4077.7 ± 222.9	3820.3 ± 114.0	3569.6 ± 136.1

Values reported as mean $\pm$ standard error.

Supplemental Table 7. Femoral neck fracture results for sitagliptin-treated and vehicle-treated control mice

	Male		Female		OVX	
	Vehicle	**Sitagliptin**	**Vehicle**	**Sitagliptin**	**Vehicle**	**Sitagliptin**
n	11	10	8	8	9	10
Structural Properties						
Ultimate Load (N)	20.4 ± 2.1	20.0 ± 1.7	21.5 ± 0.8	21.1 ± 1.5	15.9 ± 1.3	14.9 ± 1.0
Failure Displacement (mm)	0.31 ± 0.03	0.33 ± 0.02	0.21 ± 0.02	0.28 ± 0.02	0.22 ± 0.03	0.18 ± 0.01
Energy to Failure (mJ)	4.0 ± 0.6	4.0 ± 0.3	2.8 ± 0.3	3.7 ± 0.5	2.1 ± 0.4	1.6 ± 0.2
Stiffness (N/mm)	112.3 ± 5.4	102.6 ± 6.1	136.4 ± 12.7	132.3 ± 11.2	105.5 ± 10.6	99.2 ± 4.9

Values reported as mean ± standard error.

Supplemental Table 8. Vertebral Compression for sitagliptin-treated and control mice

	Male		Female		OVX	
	Vehicle	**Sitagliptin**	**Vehicle**	**Sitagliptin**	**Vehicle**	**Sitagliptin**
n	**11**	**10**	**8**	**8**	**11**	**10**
Structural Properties						
Ultimate Load (N)	30.7 ± 2.5	30.2 ± 2.3	25.8 ± 2.5	25.3 ± 2.9	19.9 ± 2.1	15.1 ± 1.8
Failure Displacement (mm)	0.31 ± 0.02	0.35 ± 0.03	0.42 ± 0.07	0.42 ± 0.08	0.37 ± 0.05	0.39 ± 0.05
Energy to Failure (mJ)	5.4 ± 0.5	6.0 ± 0.4	6.9 ± 1.4	6.5 ± 1.2	4.3 ± 0.8	3.7 ± 0.6
Stiffness (N/mm)	161.3 ± 17.0	149.2 ± 19.2	113.3 ± 11.1	87.4 ± 13.1	108.8 ± 17.6	76.5 ± 13.0
Material Properties						
Ultimate Stress (MPa)	13.7 ± 1.1	12.8 ± 1.1	10.3 ± 1.1	10.8 ± 1.3	9.3 ± 0.9	6.4 ± 0.8
Failure Strain (%)	10.4 ± 0.6	11.2 ± 0.9	13.1 ± 2.2	12.5 ± 2.0	11.9 ± 1.6	12.6 ± 1.8
Toughness (MPa)	0.81 ± 0.07	0.83 ± 0.07	0.87 ± 0.18	0.86 ± 0.18	0.64 ± 0.12	0.50 ± 0.08
Young's Modulus (MPa)	211.3 ± 20.8	192.9 ± 24.6	145.9 ± 15.8	123.7 ± 18.5	162.9 ± 29.18	105.6 ± 19.1*

*Values reported as mean ± standard error. * Significant (p ≤ 0.05) compared to vehicle-treated control mice*

Supplemental Table 9. Osteoclast staining results for sitagliptin-treated and control mice

	Male		Female		OVX	
	Vehicle	**Sitagliptin**	**Vehicle**	**Sitagliptin**	**Vehicle**	**Sitagliptin**
n	**9**	**10**	**8**	**8**	**9**	**11**
Number of Osteoclasts (-)	66 ± 6	61 ± 6	64 ± 6	53 ± 7	45 ± 4	52 ± 6
Osteoclast Surface (mm)	1.2 ± 0.1	1.1 ± 0.1	1.3 ± 0.1	1.3 ± 0.3	0.93 ± 0.11	1.5 ± 0.3
Percent Osteoclast Surface (%)	7.1 ± 1.0	6.2 ± 0.7	13.4 ± 1.8	14.0 ± 2.2	10.1 ± 1.4	12.8 ± 1.9
Number of Osteoclasts per Bone Surface (mm^{-1})	3.9 ± 0.5	3.4 ± 0.4	6.7 ± 1.0	5.7 ± 0.6	4.9 ± 0.5	4.6 ± 0.5
Number of Osteoclasts per Osteoclast Surface (mm^{-1})	56.7 ± 2.1	55.3 ± 1.0	50.5 ± 4.6	42.9 ± 2.7	52.5 ± 5.9	39.3 ± 3.8

Values reported as mean $\pm$ standard error.

Supplementary Table 10. Femoral three-point bending results for Dpp4-/- (KO) and WT mice

	Male		Female		OVX	
	WT	KO	WT	KO	WT	KO
n	14	23	14	17	10	13
Structural Properties						
Ultimate Load (N)	17.0 ± 0.6	16.2 ± 0.5	20.8 ± 0.9	20.8 ± 0.7	16.9 ± 0.7	15.5 ± 0.7
Failure Displacement (mm)	0.70 ± 0.11	0.55 ± 0.06	0.30 ± 0.04	0.41 ± 0.04	0.29 ± 0.04	0.34 ± 0.04
Energy to Failure (mJ)	7.9 ± 1.0	6.1 ± 0.6	4.3 ± 0.7	5.7 ± 0.65	3.5 ± 0.6	3.4 ± 0.5
Stiffness (N/mm)	139.3 ± 3.7	132.7 ± 5.6	165.2 ± 6.6	163.0 ± 6.8	154.7 ± 3.6	131.1 ± 6.6*
Material Properties						
Ultimate Stress (MPa)	105.6 ± 3.9	99.4 ± 4.1	147.7 ± 5.3	147.7 ± 4.8	115.8 ± 6.8	129.5 ± 7.3
Failure Strain (%)	14.7 ± 2.6	13.1 ± 1.5	6.7 ± 0.8	9.2 ± 1.0	6.6 ± 0.8	7.5 ± 1.0
Toughness (Mpa)	10.9 ± 1.5	8.7 ± 0.9	6.8 ± 1.1	9.2 ± 1.1	5.5 ± 0.9	7.0 ± 1.0
Young's Modulus (Mpa)	3889.7 ± 260.1	3534.8 ± 214.7	5253.4 ± 243.1	5141.4 ± 255.5	4546.0 ± 163.6	5028.1 ± 214.2

*Values reported as mean ± standard error. * Significant (p ≤ 0.05) compared to wildtype control*

Supplementary Table 11. Femoral neck fracture results for Dpp4-/- (KO) and WT mice

	Male		Female		OVX	
	WT	KO	WT	KO	WT	KO
n	14	23	13	16	10	13
Structural Properties						
Ultimate Load (N)	22.5 ± 0.9	22.6 ± 1.0	17.8 ± 0.8	17.5 ± 0.9	18.1 ± 0.7	13.3 ± 0.5*
Failure Displacement (mm)	0.27 ± 0.03	0.26 ± 0.02	0.23 ± 0.03	0.30 ± 0.04	0.28 ± 0.02	0.26 ± 0.02
Energy to Failure (mJ)	3.4 ± 0.3	3.2 ± 0.2	2.4 ± 0.3	3.2 ± 0.4	2.9 ± 0.2	2.1 ± 0.2*
Stiffness (N/mm)	121.7 ± 8.8	135.5 ± 9.7	115.8 ± 11.3	104.2 ± 8.8	114.5 ± 4.8	83.0 ± 4.7*

*Values reported as mean ± standard error. * Significant (p ≤ 0.05) compared to wildtype control*

Supplemental Table 12. Vertebral compression results for Dpp4-/- (KO) and WT mice

	Male		Female		OVX	
	WT	KO	WT	KO	WT	KO
n	13	21	12	19	9	13
Structural Properties						
Ultimate Load (N)	24.1 ± 2.9	17.2 ± 1.3*	17.7 ± 2.2	19.7 ± 1.6	18.6 ± 1.5	14.4 ± 2.2
Failure Displacement (mm)	0.34 ± 0.05	0.34 ± 0.09	0.36 ± 0.06	0.36 ± 0.04	0.39 ± 0.05	0.38 ± 0.05
Energy to Failure (mJ)	5.0 ± 1.0	3.8 ± 0.5	4.1 ± 0.8	4.4 ± 0.7	4.8 ± 0.9	3.9 ± 0.9
Stiffness (N/mm)	129.4 ± 20.6	83.8 ± 7.4	83.8 ± 11.3	114.1 ± 10.0	89.1 ± 10.5	74.1 ± 9.7
Material Properties						
Ultimate Stress (Mpa)	9.8 ± 1.3	7.3 ± 0.5	7.4 ± 0.9	8.5 ± 0.7	8.0 ± 0.7	6.5 ± 1.0
Failure Strain (%)	10.4 ± 1.5	10.5 ± 0.9	11.2 ± 1.7	10.1 ± 1.2	12.6 ± 1.5	12.2 ± 1.5
Toughness (Mpa)	0.62 ± 0.11	0.49 ± 0.06	0.54 ± 0.10	0.55 ± 0.09	0.68 ± 0.14	0.56 ± 0.13
Young's Modulus (Mpa)	169.1 ± 27.1	118.8 ± 11.5	113.4 ± 16.5	161.5 ± 13.9*	119.4 ± 16.2	103.2 ± 15.0

*Values reported as mean ± standard error. * Significant (p ≤ 0.05) compared to wildtype control*

Supplemental Table 13. Vertebral trabecular architecture in Dpp4-/- (KO) and WT mice

	Male		Female		OVX	
	WT	KO	WT	KO	WT	KO
n	15	23	13	16	10	13
BV/TV (%)	26.2 ± 1.4	25.2 ± 0.9	23.8 ± 1.5	20.4 ± 0.9	19.5 ± 1.3	19.1 ± 1.1
Tb.Th. (μm)	68.2 ± 0.7	65.1 ± 1.0*	66.7 ± 1.4	66.9 ± 0.9	62.1 ± 0.7	60.6 ± 0.7
Tb.N. (mm^{-1})	3.8 ± 0.2	3.9 ± 0.1	3.6 ± 0.2	2.9 ± 0.2*	3.1 ± 0.2	3.2 ± 0.2
Tb.Sp. (μm)	199.9 ± 13.1	200.2 ± 4.9	260.8 ± 18.8	272.0 ± 17.3	223.4 ± 23.0	223.4 ± 20.4

*Values reported as mean ± standard error. * Significant (p ≤ 0.05) compared to wildtype control*

Supplemental Table 14. Vertebral trabecular connectivity for Dpp4-/- (KO) and WT mice

		Male		Female		OVX	
		WT	KO	WT	KO	WT	KO
	n	15	22	13	18	10	11
Measures of Connectivity	Total Strut Length (mm/mm^2)	4.70 ± 0.22	4.63 ± 0.18	3.94 ± 0.22	3.94 ± 0.30	3.21 ± 0.20	2.99 ± 0.16
	Number of Nodes (mm^{-2})	8.8 ± 0.6	9.4 ± 0.8	10.0 ± 1.4	10.3 ± 1.6	5.9 ± 0.8	5.2 ± 0.6
	Length of Node-Node Struts (mm/mm^2)	1.21 ± 0.21	1.12 ± 0.15	1.02 ± 0.16	1.25 ± 0.22	0.78 ± 0.19	0.54 ± 0.10
	Length of Node-Free Struts (mm/mm^2)	1.57 ± 0.12	1.54 ± 0.10	1.56 ± 0.16	0.98 ± 0.07*	1.03 ± 0.10	0.94 ± 0.12
Measures of Disconnectivity	Number of Free Ends (mm^{-2})	15.3 ± 0.8	14.9 ± 0.6	14.7 ± 1.7	12.9 ± 1.0	10.6 ± 0.4	10.5 ± 0.4
	Length of Free-Free Struts (mm/mm^2)	0.60 ± 0.08	0.67 ± 0.08	0.49 ± 0.05	0.56 ± 0.07	0.46 ± 0.05	0.51 ± 0.07

*Values reported as mean ± standard error. * Significant (p ≤ 0.05) compared to wildtype control*

Supplemental Table 15. Osteoclast staining for Dpp4-/- (KO) and WT mice

	Male		Female		OVX	
	WT	KO	WT	KO	WT	KO
n	9	9	8	13	9	13
Number of Osteoclasts (-)	55 ± 6	43 ± 5	74 ± 10	60 ± 4	51 ± 5	55 ± 5
Osteoclast Surface (mm)	0.89 ± 0.15	0.60 ± 0.08	1.1 ± 0.2	0.93 ± 0.06	0.96 ± 0.13	0.91 ± 0.07
Percent Osteoclast Surface (%)	5.6 ± 0.8	3.9 ± 0.4	8.6 ± 1.4	8.3 ± 0.9	7.3 ± 0.7	7.6 ± 0.6
Number of Osteoclasts per Bone Surface (mm^{-1})	3.6 ± 0.4	2.8 ± 0.3	5.9 ± 0.9	5.3 ± 0.4	4.0 ± 0.4	4.5 ± 0.3
Number of Osteoclasts per Osteoclast Surface	66.7 ± 3.8	72.7 ± 2.7	69.7 ± 2.9	65.4 ± 2.0	59.5 ± 2.1	60.2 ± 2.0

Values reported as mean ± standard error
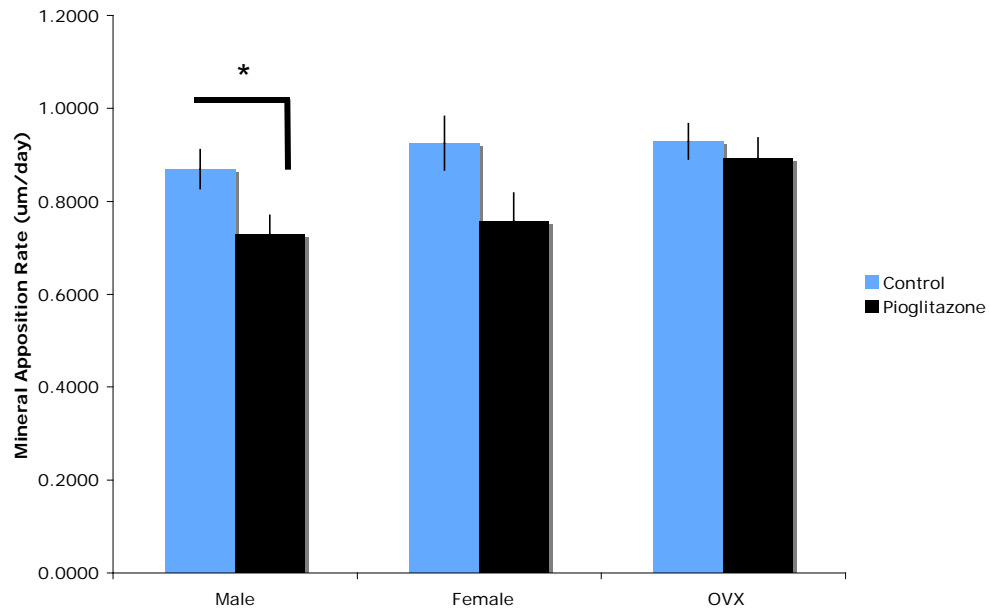
Supplemental Figure 1

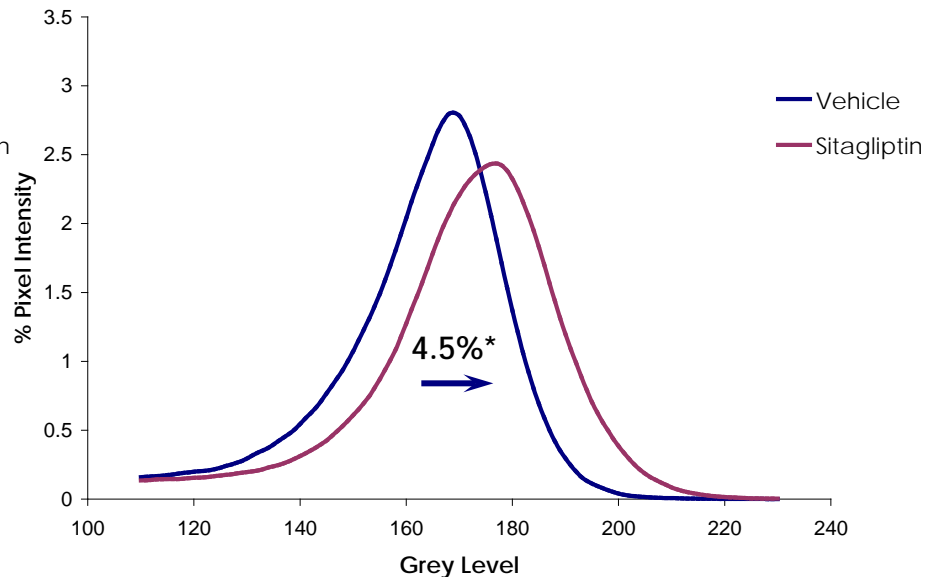Mineral apposition rate for male, female, and OVX HFD mice treated with vehicle or pioglitazone*= p<0.05
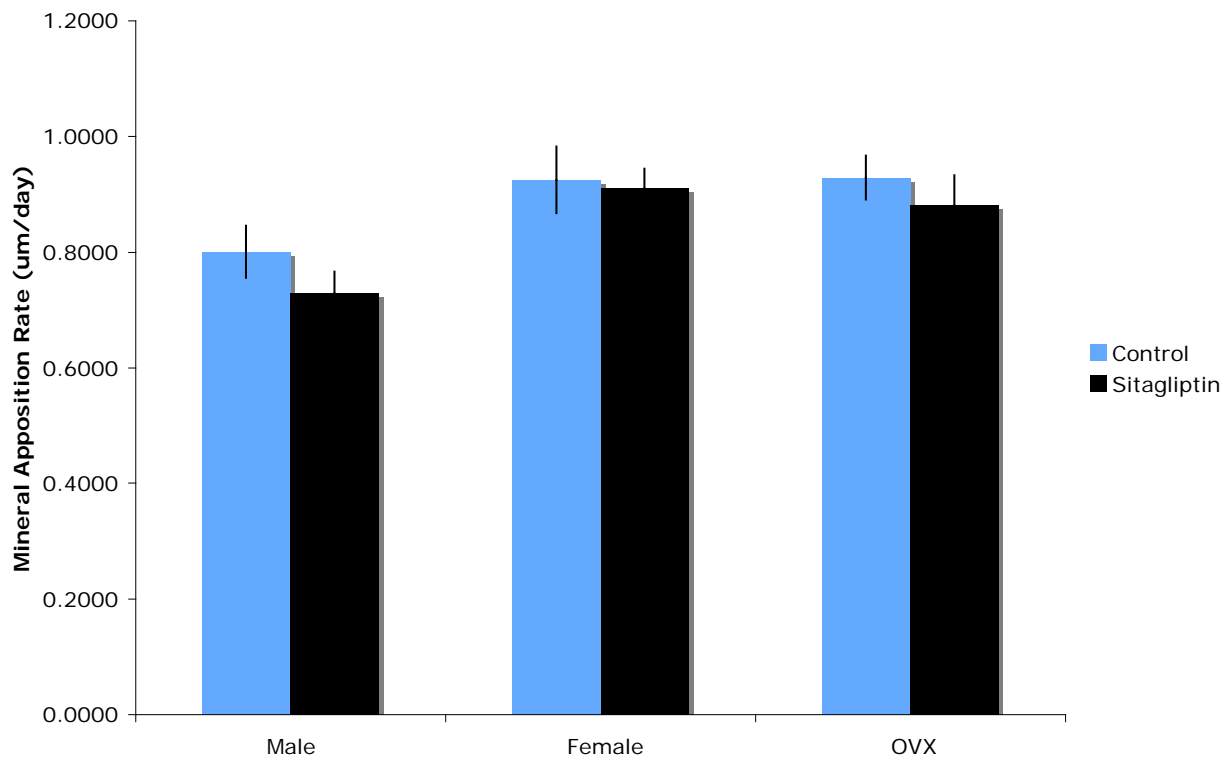
Supplementary Figure 2

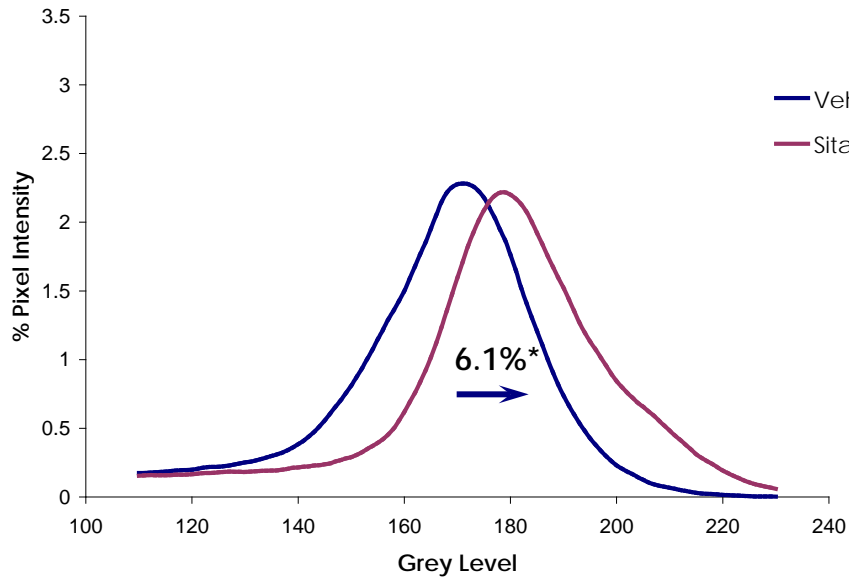Mineral apposition rate for male, female, and OVX HFD mice treated with vehicle or sitagliptin *= p<0.05

Trabecular Mineralization Profiles of Male Mice
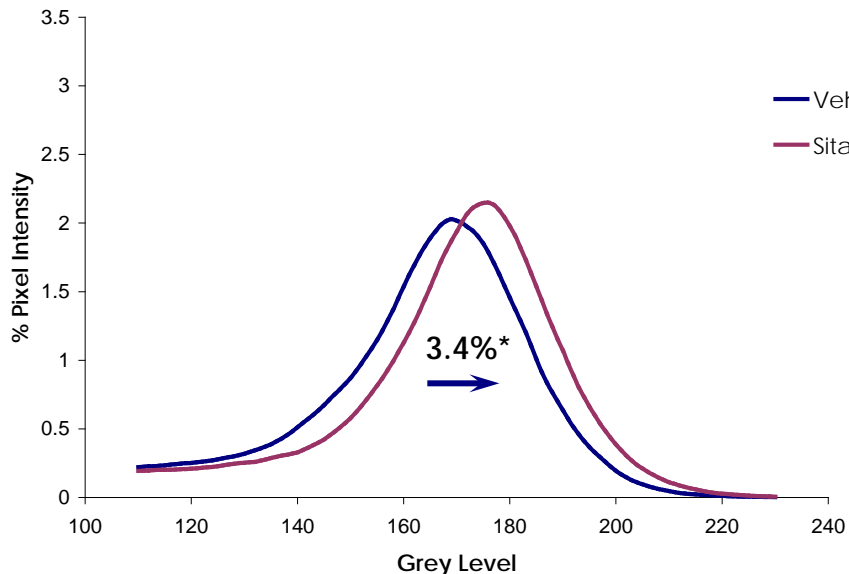
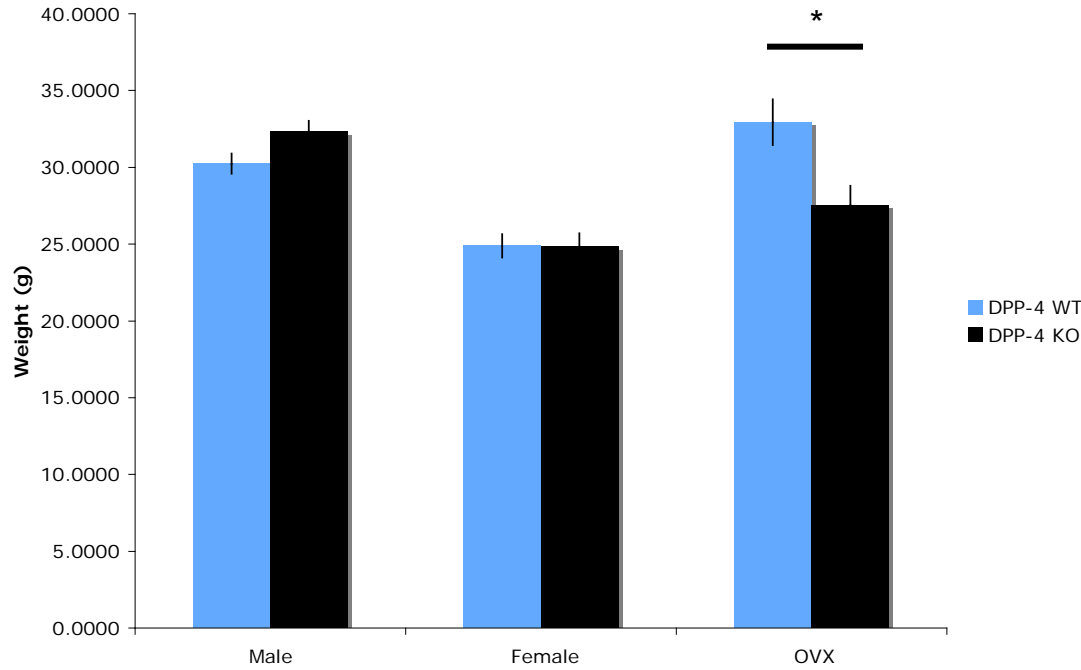**Trabecular Mineralization Profiles of Female Mice**

Trabecular Mineralization Profiles of OVX Mice

Average mineralization profiles for trabecular
bone area in sitagliptin- vs. vehicle-treated HFD mice
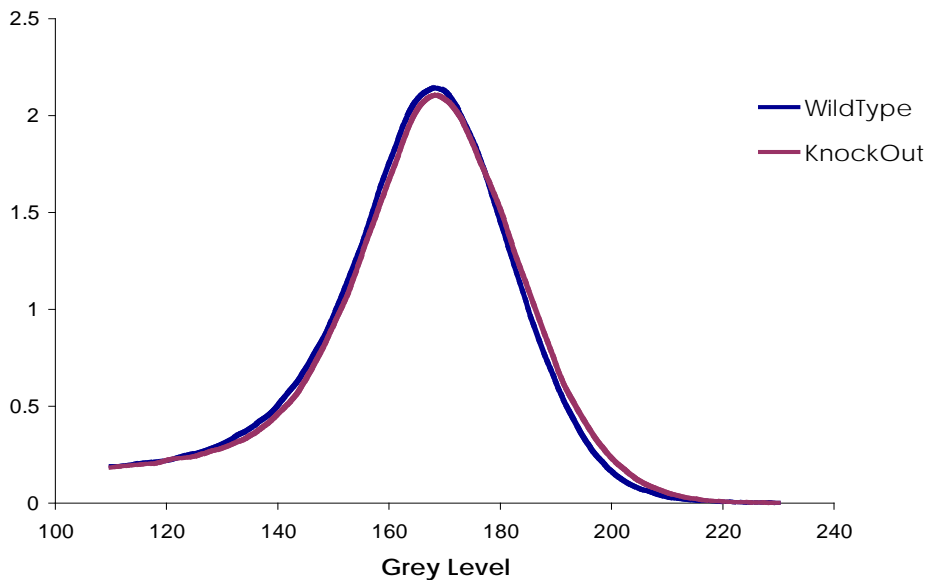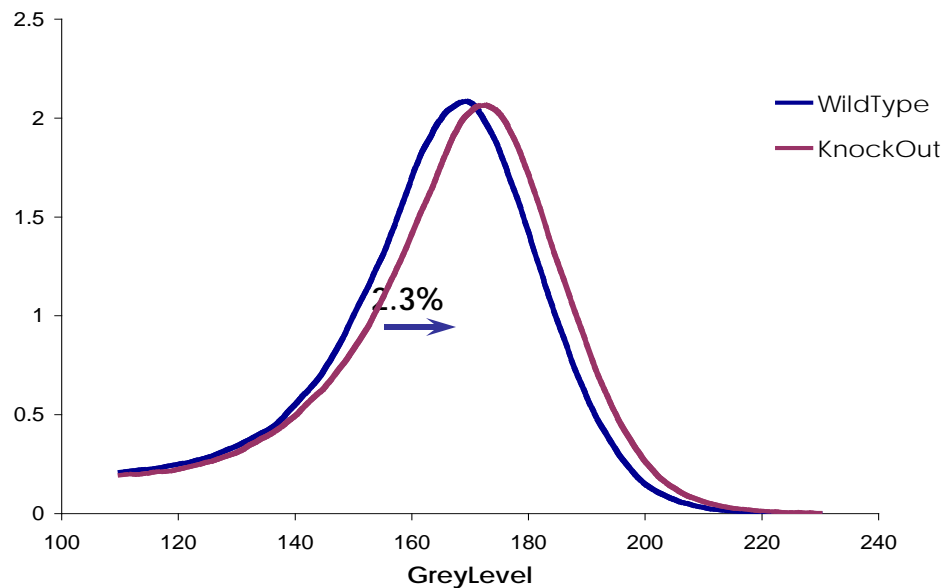* = p< .05 vehicle vs. sitagliptin

Supplementary Figure 3

Body weight in *Dpp4*+/+ and *Dpp4*-/- mice

Supplementary Figure 4

Body weight in male and female littermate *Dpp4*+/+ and *Dpp4*-/- 7 month old mice * = p<.05, DPP-4 WT vs. DPP-4 KO

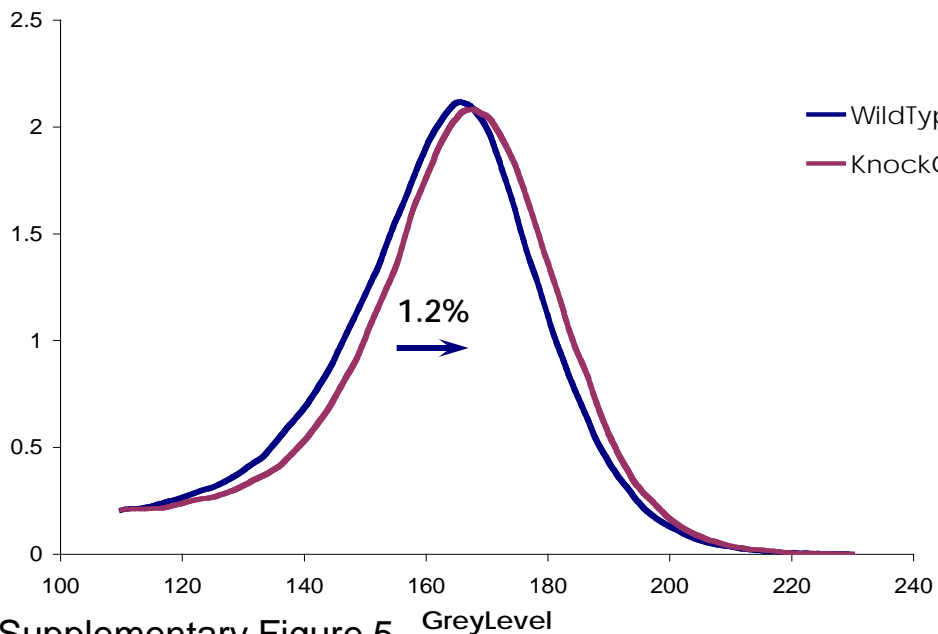**Trabecular Mineralization Profiles of Male Mice**

Trabecular Mineralization Profiles of Female

Trabecular Mineralization Profiles of OVX Female Mice

Average mineralization profiles for trabecular bone area in *Dpp4*+/+ and *Dpp4*-/- mice

Supplementary Figure 5

Supplementary Figure 6   Mineral apposition rate in male, female and OVX Dpp4+/+ (WT) and Dpp4-/- (KO) mice